PCCP

Accepted Manuscript

ROYAL SOCIETY OF CHEMISTRY

www.rsc.org/pccp

Hydrogen adsorption on bimetallic PdAu(111) surface alloys: Minimum adsorption ensemble, ligand and ensemble effects, and ensemble confinement

Naoki Takehiro[1,a], Ping Liu[2,b], Andreas Bergbreiter[1,c], Jens K. Nørskov[2,d], R. Jürgen Behm[1],*

[1]Inst. of Surface Chemistry and Catalysis, Ulm University, D-89069 Ulm, Germany

[2]Dept. of Physics, Technical University of Denmark, Building 307, DK-2800 Lyngby, Denmark

Abstract

The adsorption of hydrogen on structurally well defined PdAu/Pd(111) monolayer surface alloys was investigated in a combined experimental and theoretical study, aiming at a quantitative understanding of the adsorption and desorption properties of individual PdAu nanostructures. Combining the structural information obtained by high resolution scanning tunneling microscopy (STM), in particular on the abundance of specific adsorption ensembles at different Pd surface concentrations, with information on the adsorption properties derived from temperature programmed desorption (TPD) spectroscopy and high resolution electron energy loss spectroscopy (HREELS) allows conclusions on the minimum ensemble size for dissociative adsorption of hydrogen and on the adsorption energies on different sites active for adsorption. Density functional theory (DFT) based calculations give detailed insight into the physical effects underlying the observed adsorption behavior. Consequences of these findings for the understanding of hydrogen adsorption on bimetallic surfaces in general are discussed.

Keywords: Bimetallic catalysts, site selective adsorption, surface chemistry, ligand/ensemble effect, STM, DFT

Submitted to Phys. Chem. Chem. Phys: 11.06.2014

[a] Current address: Toyota Motor Corporation, Higashifuji Technical Center, 1200 Mishuku, Susana, Shizuoka 410-1193 (Japan)
[b] Current Address: Department of Chemistry, Brookhaven National Laboratory, Building 5555, Upton NY 11973 (USA)
[c] Current address: Carl Zeiss SMT GmbH, Rudolf-Eber-Straße 2, D-73447 Oberkochen (Germany)
[d] Current address: Stanford University and SUNCAT Center for Interface Science & Catalysis, SLAC National Accelerator Laboratory, Menlo Park, CA 94025 (USA)
* Author to whom correspondence should be addressed: email: juergen.behm@uni-ulm.de

1 Introduction

Bimetallic surfaces have been studied intensely using surface science techniques to identify the physical origin of the often superior catalytic properties of bimetallic catalysts as compared to their respective constituents, but also with respect to monometallic supported catalysts in general, on an atomic scale.[1] The level of insight gained from these model studies has increased dramatically with the advances in structural characterization, in particular by high resolution scanning tunneling microscopy (STM), e.g., for the resolution and chemical identification of different metal surface atoms [2-4] and progress in the theoretical description of adsorbates and surface reactions.[5-8] Using tailored nanostructured surfaces with well known concentrations of individual structural elements ('nanostructures'), one ultimately aims at a qualitative and quantitative understanding of the chemical and catalytic properties of these nanostructures. This, in turn, can be used for designing optimized surfaces and finally optimized catalysts. The power and potential of such approaches has been demonstrated for various reactions.[9-11] One example was the vinyl acetate synthesis on PdAu catalysts, which had been investigated in detail by Goodman and coworkers, both on dispersed catalysts and on model surfaces.[12-17] For a better understanding of the chemistry of these PdAu surfaces, we had studied the interaction of different, structurally well characterized PdAu surfaces such as Au monolayer island modified Pd(111) surfaces or PdAu/Pd(111) monolayer surface alloys with CO, using this as probe molecule.[18-20]

Extending our previous study, we here report on the interaction of hydrogen with bimetallic PdAu/Pd(111) surface alloys. First results had been included in an earlier review.[21] We are specifically interested in identifying active Pd ensembles for stable hydrogen adsorption, in particular the minimum Pd ensemble size for hydrogen adsorption, but equally in a semi-quantitative understanding of the nature and contributions of the different electronic and geometric effects affecting hydrogen adsorption on these bimetallic surfaces, such as

electronic ligand [22-24] and strain effects [25] as well as geometric ensemble effects.[24,26,27]

Before presenting and discussing the results, we will briefly summarize earlier findings relevant for this study. Hydrogen adsorption on Pd(111) has been studied intensely. Most important for the present study is that hydrogen adsorbs dissociatively with a high sticking coefficient on threefold hollow sites, with adsorption energies differing between 1 eV [28] and 1.48 eV.[29] In addition, a subsurface adsorption site was identified, which can be populated upon adsorption at 120 – 150 K. Desorption from these sites occurs at around 200 K.[30-32] For adsorption at low temperatures (≤120 K), population of this site is kinetically inhibited.[30]

Much less is known about hydrogen adsorption on Au(111), assuming this as model for the other constituent of the surface alloy.[33] Au is known to be essentially inert towards dissociative hydrogen adsorption,[34] and DFT calculation have shown for Au(111) that this refers both to thermodynamics, where H_2/Au(111) is one of the few chemisorption systems for which H_2 in the gas phase is energetically favored compared to adsorbed atomic hydrogen (H_{ad}), and to kinetic effects, because of a pronounced barrier for dissociative adsorption desorption.[33] As a result, atomic hydrogen adsorbed on Au is metastable against instantaneous recombinative desorption.

For CO adsorption on bimetallic PdAu surfaces, we derived the adsorption properties of different Pd_n ensembles on PdAu/Pd(111) monolayer surface alloys in a combined experimental and theoretical study.[20] Employing temperature programmed desorption (TPD), high resolution electron energy loss spectroscopy (HREELS) and high resolution STM as well as density functional theory (DFT) based calculations, and correlating the appearance of spectroscopic features with the abundance of certain structural elements, we determined distinct ensemble effects in CO adsorption. A single Pd surface atom surrounded by Au atoms was found to adsorb one CO molecule on the atop site, but with a significantly lower

adsorption energy than on Pd(111) (T_{des} ≈ 300 K), while a Pd dimer allows for stronger adsorption on a Pd_2 bridge site. Strongest adsorption, which resembles that on Pd(111), was found for CO adsorption on threefold hollow sites above a compact Pd_3 trimer or larger ensembles with Pd_3 sites. These experimental findings were confirmed and rationalized by DFT calculations.[20]

Those results agree well with findings of Goodman and coworkers, who equally investigated this system by CO-TPD and vibrational spectroscopy, using multilayer PdAu alloy films with thicknesses of >10 monolayers deposited on a Mo(110) substrate as model surface.[15,17] In their case, the surface composition was quantified by ion scattering spectroscopy (ISS).[12,35]

Ligand and ensemble effects in the adsorption of CO, O and N on PdAu/Pd(111) monolayer surface alloys had been investigated and disentangled in a theoretical study by Liu and Nørskov.[36] The first report on the catalytic activity of PdAu catalysts in different reactions was published by Eley.[37] Baddeley et al. investigated the cyclization of acetylene on PdAu/Pd(111) surface alloys.[38,39] Vinyl acetate synthesis on PdAu catalysts had been investigated in detail by Goodman and coworkers, both on dispersed catalysts and on model surfaces.[12] The hydrogenation of oxygen on PdAu/Pd(111) surface alloys was investigated by DFT calculations by Ham et al.,[40,41] closely related to the observation of highly selective H_2O_2 formation on supported PdAu catalysts.[42,43] Neurock and Mei reported results of a combined DFT and Monte Carlo study on the hydrogenation of ethylene on PdAu(111) alloy surfaces with different compositions, focusing on the role of Au in that reaction.[44]

The interaction of bimetallic PdAu surfaces with hydrogen was investigated also by electrochemical methods. In this case, the surfaces were created either by diffusion controlled *in situ* co-deposition of Pd and Au on a Au(111) substrate, which leads to a PdAu/Au(111)

surface alloy, or by electrochemical deposition of a thick (ca. 20 ML) PdAu film on a Ru(0001) substrate and subsequent heating at 700°C,[45] or by pulse deposition of Pd clusters on Au(111).[46-48] Based on combined *in situ* STM and electrochemical measurements, Maroun et al. determined that Pd dimers must be active for underpotential H adsorption, by comparing the abundance of different Pd_n surface elements and the charge of the H_{upd} adsorption peak.[49] Pluntke et al. concluded that a Pd monomer on a Au film must be active for H_2 evolution, assuming a similar surface composition as derived by Goodman and coworkers for comparable systems prepared in vacuum.[45] Stimming and coworkers reported that Pd clusters on a Au electrode enhance the H_2 evolution rate by more than 2 orders of magnitude and explained this by thickness dependent strain effects in the Pd structure.[46-48,50] Related to this work, Roudgar et al. calculated that three-dimensional Pd_9 clusters on a Au(111) surface interact less strongly with adsorbates than a pseudomorphic Pd overlayer.[51-53]

In the following, we will, after a brief description of the experimental set-up and procedures and of computational details, first evaluate the structure of the PdAu/Pd(111) surface alloys, as derived from STM imaging (section 3.1), then present TPD and HREELS measurements on different surface alloys (section 3.2), and finally the results of the DFT calculations and their correlations with the experimental findings, in particular with the trends in adsorption energies on different PdAu nanostructures and their ability to adsorb hydrogen (section 3.3). Here we will also discuss consequences of these findings for the understanding of hydrogen adsorption on bimetallic surfaces in general.

2 Experimental and Calculational Details

2.1 Experimental Details

All experiments were carried out in an ultrahigh vacuum (UHV) chamber with a base pressure below 10^{-10} mbar, which was equipped with a variable temperature STM and

facilities for surface preparation and characterization. The latter include a differentially pumped mass spectrometer for TPD measurements, as well as spectrometers for HREELS and X-ray photoelectron spectroscopy (XPS), and a low energy electron diffraction (LEED) system.[18] The mass spectrometer was covered by a Au coated snout with an aperture of 2 mm in diameter.[54] The distance between the aperture and the sample was fixed to less than 1 mm by a spacer. The sample temperature was ramped at 20 K s^{-1} during TPD measurements. The sample was flushed to 600 K before D_2 exposure at ≤120 K to remove trace amounts of adsorbates from the residual gas.

The Pd(111) crystal was cleaned by repeated cycles of Ar ion bombardment, annealing in O_2 at 700 K, and annealing to 1250 K. The crystal was judged clean based on XPS and STM measurements. Au was evaporated from a Au droplet on a W wire heated resistively. The amount and purity of evaporated Au were checked by XPS and STM.

From technical reasons the interaction with hydrogen was investigated using deuterium adsorption, because of the much lower D_2 background pressure in the UHV system. For D_2 exposure, a tube doser was used to reduce the exposure of the sample surroundings. To avoid confusion with calculations and other studies, we will generally use the term 'hydrogen', and only refer to deuterium in the context of experimental details.

2.2 Computational details

DFT calculations were based on the DFT-GGA, which was implemented in the DACAPO code.[55] The Kohn-Sham one electron valence state was solved on a basis of plane waves with kinetic energies below 25 Ry and an ultra soft pseudopotential was used.[56] The exchange-correlation energy and potential were described by the revised Perdew-Burke-Ernzerhof (RPBE) functional.[57] The optimized lattice constants for Pd (3.91 Å) and Au (4.10 Å) bulk agree well with experimental values (3.89 Å for Pd and 4.07 Å). The adsorption energy of

hydrogen was defined as $E_{ad} = \frac{2}{n}[E(nH/surf) - E(surf)] - E(H_2)$, where n is the number of H atoms adsorbed on the surface. In all cases, hydrogen was allowed to relax in all directions. The PdAu/Pd(111) systems were described by substituting Pd atoms in the top layer gradually by Au at lattice position, where the modeling of the surfaces were performed at two different levels. For elucidating trends, in particular for evaluating ligand and ensemble effects, the surface systems were described by using a three-layer slab of Pd (111) with a (2×2) or (3×3) supercell on each layer, while metal atoms were fixed at the lattice position of the substrate. Different sites were selected for hydrogen adsorption (see Figures). Further details on such calculation were given in [36]. For quantitative calculation of adsorption energies on an absolute scale we additionally performed calculations using a five-layer metal slab in a (3×3) or (3×4) unit cell, where the upper two metal layers were allowed to relax with hydrogen, while the k-points were kept the same as in the previous calculations. We have checked that the relaxation of the top two layers indeed changes the adsorption energy, but the trend in variation from one system to the next remained the same. In selected cases activation energies for dissociative adsorption were calculated employing the Linear Synchronous Transit (LST) method to bracket the maximum between the reactants and products,[58] followed by repeated conjugate gradient minimizations and the Quadratic Synchronous Transit (QST) maximizations until a transition state was located. The convergence thresholds were set as that the root mean square (rms) forces on the atoms were smaller than 0.01 eV/Å. Such methods yield results close to those obtained by eigenvector following methods.

3 Results and Discussion

3.1 Structure of PdAu/Pd(111) surface alloys

The PdAu/Pd(111) surface alloys were prepared by evaporating one to two layers of Au

on the Pd(111) surface at room temperature, which grow in a layer-by-layer mode.[54] Annealing these samples to 750 - 850 K, which is just sufficient to start exchange processes at the Au – Pd(111) interface and Au dissolution, leads to the formation of bimetallic Pd-Au surfaces with different surface compositions, where the density of Pd atom in the topmost layer increases upon increasing the annealing temperature.[20,54] It should be noted that neither in this work nor in a preceding study we had any evidence for a surface reconstruction.[20] The distribution of the atoms in the surface layer was derived by quantitative evaluation of series of atomic resolution STM images for each surface concentration, which allowed to distinguish between Pd and Au surface atoms by the so called 'chemical contrast'.[59] Representative STM images, where due to electronic effects Pd surface atoms appear bright and Au surface atoms are dark, are presented in Fig. 1. First of all, these images clearly demonstrate that the two different types of atoms are homogeneously distributed in the topmost layer. For the lowest Pd surface concentration (3.5% Pd, Fig. 1a) in the images in Fig. 1 we find only Pd monomers in the surface layer, while for the next higher concentration (12.5% Pd) Pd monomers and dimers are present (Fig. 1b). Only when reaching Pd surface concentrations of above 20% (23% Pd, Fig. 1c), also compact and linear trimers appear, although at rather low concentrations. The high Pd concentration in Fig. 1d (78% Pd) essentially reflects the reverse situation, with largely Au monomers and dimers and some larger Au aggregates.

Based on results of preliminary deuterium adsorption experiments we focused on Pd surface concentrations in the range between 20% and 40%, where not only Pd monomers and dimers are present, but also larger Pd_n ensembles (see also section 3.2) and where the differences between different models for the minimum size ('critical size') of the adsorption ensemble and its composition will be most pronounced. Quantitative evaluation of the STM images of the surface alloys employed for the adsorption experiments in the present study yielded the distributions of different ensembles and ensemble sizes given in Table I and in

Fig. 2. Considering that in the end we want to correlate the abundance of different adsorption sites with the TPD spectra, we did not list the relative abundance of specific ensemble sizes, but of specific adsorption sites, such as Pd_2 dimer sites etc., independent of whether they occur in a Pd dimer or in a larger Pd ensemble (Table 1). The same holds true for Pd_3 sites. The quantitative evaluation of sets of STM images obtained for $Pd_{21}Au_{79}$/Pd(111), for $Pd_{28}Au_{72}$/Pd(111) and for $Pd_{38}Au_{62}$/Pd(111) confirmed the qualitative impression derived from the images in Fig. 1, that monomers and dimers are dominant up to Pd surface concentrations of 20%. In addition to Pd_1 sites, we give the concentration of Pd_2 bridge sites and of Pd_3 as well as that of Pd_2Au threefold hollow sites, and finally also of compact Pd_4 tetramer sites. $PdAu_2$ sites were not evaluated, since their surface concentration is much too high to account for the desorption in the low temperature β_1 peak of the D_2-TPD spectra recorded on the PdAu surface alloys (see next section). Furthermore, the calculations (section 3.3) will show that the adsorption energies on these sites are much too low to stabilize adsorbed hydrogen at the present adsorption temperature. The remaining sites in Table 1 will be discussed later, in combination with the D_2-TPD data and the results of the calculations. The populations of other sites with different compositions, up to pentamers, is illustrated in Fig. 2.

It should be noted that within the statistical accuracy in determining the ensemble size distribution for Pd monomers, Pd_2 and PdAu dimers, Pd_xAu_{3-x} trimers, Pd_xAu_{4-x} tetramers and Pd_xAu_{5-x} pentamer sites this essentially corresponds to a calculated statistical (random) distribution the Pd surface atoms. The latter is indicated by the dashed lines in Fig. 2. While the number of Pd surface concentrations investigated is too low for a conclusive statement, the data provide at least clear evidence that at the freezing temperature of the surface alloy, i.e., at the temperature where surface diffusion becomes too slow to reach the equilibrium configuration during cool down, effective mutual interactions between the different surface

species play do not significantly affect the distribution of surface atoms.[60] This result fits well to the miscibility of PdAu alloys, furthermore it allows us to estimate ensemble size distributions also for other Pd surface concentrations in this range of Au surface concentrations assuming a statistical distribution of surface atoms.

Finally, for comparison with the TPD experiments it is important to note that the composition and the ensemble size distribution of the topmost layer showed no change before and after the TPD experiments.

3.2 Adsorption and desorption of hydrogen on PdAu/Pd(111) surface alloys

The interaction of hydrogen with these surfaces was characterized by D_2-TPD measurements. A series of D_2-TPD spectra recorded after increasing D_2 exposures to a $Pd_{37}Au_{63}$/Pd(111) surface (adsorption temperature 110 - 120 K) is shown in Fig. 3. The spectra clearly resolve two distinct desorption peaks with a maximum at 235 K (β_1 peak) and a shoulder at 325 K (β_2 peak). The additional desorption at higher temperatures (> 450 K), which is very low on an absolute scale, is attributed to background desorption, e.g., from the sample holder. The origin of the β_1 and β_2 states, which in general may arise either from differences in the adsorption energies, or more correctly, in the activation energy for desorption, or from repulsive interactions between the D_{ad} species, will be discussed later. It should also be noted that neither STM imaging nor comparison of TPD spectra before and after such series gave any indication for H_{ad} induced modification of the surface such as Pd segregation in these experiments.

Most important feature in the spectra is the characteristic coverage dependence in the desorption peaks. Different from the second order desorption kinetics normally observed for recombinative hydrogen desorption, the maxima do not shift to lower temperatures with increasing coverage, but remain at essentially constant temperature. This is most easily

explained by 'direct' desorption from the individual ensembles, where surface diffusion of D_{ad} species between different Pd_n ensembles is inhibited, i.e., the D_{ad} species are confined to the Pd_n ensemble where they were adsorbed, and the small size of these ensembles. In that case, an increasing D_{ad} coverage results in an increasing number of Pd_n ensembles populated with D_{ad} species, without modifying the local coverage on these Pd_n ensembles. This way, the desorption characteristics remain constant for increasing D_{ad} coverage, only the total intensity increases.

These desorption characteristics also explain a second uncommon feature, namely the population of the low-temperature state before the more stable high temperature state is filled. In fact, the overall shape of the spectra changes very little with increasing D_{ad} coverage, and the low-temperature β_1 peak is higher in intensity than the β_2 peak from the lowest coverage on. As described above, in the absence of D_{ad} surface diffusion the respective desorption states are populated for each Pd_n ensemble separately. This also indicates that the states are characteristic for dissociative adsorption of a single D_2 molecule per Pd_n ensemble, where only larger ensembles may contain more adsorbed deuterium. It should be noted that a coverage independent peak temperature could also be obtained if desorption is induced by a structural transition of the surface, which, however, is in contrast to STM observations.

The evolution of the desorption spectra with increasing Pd surface concentration is illustrated in Fig. 4, which shows TPD spectra recorded upon saturation with deuterium for three bimetallic surfaces with different Pd surface contents (21%, 28%, and 38%) and, for comparison, of a Pd(111) surface. The latter TPD spectrum closely resembles Pd(111) saturation spectra reported in earlier studies, with a slightly asymmetric peak shape and a peak temperature of about 325 K.[30,61,62] It is important to note that the D_2-TPD spectrum recorded on Pd(111) does not show any desorption from subsurface sites, in agreement with

expectations for the low adsorption temperature.[30,32] The latter would result in a desorption peak at ~200 K, which would interfere with the low-temperature β_1 peak induced by Au on the surface.

The D_2-TPD spectra illustrate that very low D_{ad} saturation coverages are obtained on the bimetallic surfaces despite the significant Pd surface contents. Contributions from background desorption were determined recording a D_2-TPD spectrum on a Pd(111) surface fully covered with a Au film and removed by subtraction from the experimental spectra. The spectra recorded on the other bimetallic PdAu surfaces exhibit the same characteristics as described for $Pd_{37}Au_{63}$/Pd(111), with a low-temperature peak at 240 – 250 K and a shoulder at 320 K. For 21% surface Pd content, this peak appears at 250 K; with increasing Pd concentration it shifted to slightly lower temperatures, reaching 235 K for the $Pd_{37}Au_{63}$/Pd(111) surface. The D_2 exposures were chosen such that the β_1 peak was saturated.

For gaining more information on the adsorption site and on the critical Pd_n ensembles size we compare the abundance of different adsorption sites and ensembles as derived from the STM images with the intensity of the β_1 TPD peak for the different Pd surface concentrations. Normalizing this to the integrated desorption intensity obtained on the Pd(111) surface (1 ML), we yield saturation coverages of 1.2±0.3% (21% Pd surface atoms), 6.0±1.0 % (28% Pd surface atoms), and 15.9±1.5 % (38% Pd surface atoms) of the saturation coverage on Pd(111), respectively, on the above surface alloys (Table 1, line 18). Due to the very low intensities in the β_2 peak after background subtraction, which led to rather large relative errors in the related hydrogen coverage due to uncertainties in the background determination, a similar quantitative evaluation was not pursued for this peak. Already from a simple comparison of the β_1 desorption peak intensities and the abundance of the different adsorption ensembles on these surfaces (see Table 1, lines 1, 2, 7, 12, 15) it is clear that the

concentrations of Pd_2 dimer sites and in particular of Pd monomer sites are far too high in the range of lower Pd concentrations to be considered as stable adsorption sites for adsorbed hydrogen. On the other hand, the number of Pd_3 threefold hollow sites and especially of compact Pd_4 tetramer sites (see section 3.3) is too low to explain the experimentally observed desorption intensity in the β_1 peak. Before discussing this in more detail, we will first present additional experimental data.

Further information on the nature of the critical Pd_n ensemble comes from HREEL spectra recorded on the $Pd_{38}Au_{62}$ surface after exposure to 4 L of H_2 (1 L = 1.33×10^{-6} mbar s), which are shown in Fig. 5. A spectrum recorded at 120 K (Fig. 5a) shows vibration losses at 96 and, much weaker, at 131 meV, which are rather close to the loss features at 96 and 125 meV reported by Conrad et al. for hydrogen adsorption on Pd (111).[63] Accordingly, these losses are assigned to the parallel and vertical vibrational mode of hydrogen on threefold hollow Pd_3 sites. Other loss peaks (227, 237 and 259 meV), whose intensity increased with increasing data acquisition time, are assigned to the C-O stretch mode of CO adsorbed on various Pd sites, which is accumulated from the residual gas.[18]

Spectra recorded at room temperature (Fig. 5b) also showed a loss peak at 96 meV, indicating that also under these conditions there are H atoms adsorbed on the Pd_3 threefold hollow sites of the $Pd_{38}Au_{62}$ surface. In addition to the H_{ad} related feature, the spectra showed an additional loss peak at 42 meV (M-CO stretch [18]). The weak signal at 131 meV and the signal at 259 meV do not appear at room temperature. The disappearance of the 259 meV signal is easily explained by the weak adsorption energy of CO adsorbed on Pd atop sites, e.g., on Pd monomers.[18] The absence of the weak signal at 131 meV, which we related to an H_{ad} band, is most easily explained by the lower H_{ad} coverage under these conditions, possibly in combination with a change in the vibrational cross section.[63]

Finally, we performed CO titration experiments on the $Pd_{21}Au_{79}$ surface (Fig. 6), exploiting the known adsorption and desorption behavior of CO, with CO adsorbed atop on a Pd monomer desorbing at 330 K, bridge bound CO_{ad} on Pd dimers desorbing at 380 K (Fig. 6a) and CO adsorbed on the threefold hollow sites above compact Pd trimers at 470 K.[20] For the present experiments, we first exposed the surface to CO at 140 K, and then annealed the sample to defined temperatures. This way, only specific Pd ensembles and sites remained CO_{ad} populated. After cooling the sample to 120 K and exposing it to D_2, we monitored the D_2 desorption. The CO exposure (0.5×10^{-6} mbar s) was set to the minimum amount that completely suppresses D_2 desorption (Figs. 6b, for the β_2 peak see below). The resulting CO TPD spectrum (Fig. 6a) clearly indicates that only Pd monomer and Pd_2 dimer sites are populated on this surface, desorption from Pd_3 hollow sites in larger Pd ensembles is absent. Furthermore, the spectra underline that similar to our previous finding (see above), the higher temperature β_2 desorption peak on this sample is largely due to background desorption, since stepwise removal of CO_{ad} causes little modification of this desorption peak. Removal of the CO_{ad} from the atop sites on Pd monomers by annealing the CO_{ad} covered surface to 330 K before post-adsorption of deuterium causes no change in the D_{ad} population (Fig. 6c), i.e., deuterium adsorption is still completely blocked. Annealing to 360 K, which causes complete desorption of atop adsorbed CO_{ad} species and some desorption of bridge bound CO_{ad}, leads to the appearance of the low-temperature β_1 D_2 desorption peak, though only with low intensity. Annealing to higher temperatures before subsequent D_2 adsorption causes the β_1 peak to grow, until after annealing to 400 K it has regained its full intensity. Main messages of this sequence are that i) Pd ensembles leading to bridge bonded CO_{ad} are active for hydrogen adsorption, in contrast to sites allowing only Pd atop adsorption, and that ii) these hydrogen species desorb in the β_1 peak, confirming our above assumption.

Based on the experimental findings discussed above we can set up a model for hydrogen adsorption on the bimetallic PdAu/Pd(111) surfaces. First we will assume that adsorbed hydrogen is localized at the Pd_n ensembles upon adsorption,[49] and that spill-over of H adatoms from one Pd_n ensemble to another one is kinetically inhibited because of the very weak H-Au bond. As will be rationalized and discussed in more detail in section 3.3, it is energetically more favorable for two H adatoms adsorbed on one Pd_n ensemble to recombine and desorb as H_2 rather than that one of them migrates to Au_3 sites, which is necessary for the H adatom to get to another, neighbored Pd_n ensemble. Hence, H adatoms are confined to the Pd_n ensemble they were adsorbed at. One important consequence of the confinement of the H_{ad} species to the original Pd_n adsorption ensemble is that each of these ensembles can accommodate only an even number of H adatoms (pairwise adsorption, Table 1, lines 5, 6, 10, 11, 14). Accordingly, we assume that adsorption of a H_2 molecule is only possible if two (additional) H adatoms can be accommodated on that ensemble. This means that even if adsorption of one H_{ad} on a Pd_2 bridge site or on a Pd_2Au hollow site is energetically stable, adsorption would only occur if adsorption of two H_{ad} is sufficiently stable.

Second, it is reasonable to assume that a Pd dimer can stabilize only one H_{ad}, either on a Pd_2 bridge site or on a Pd_2Au hollow site, meaning that occupation of two directly neighbored fcc and hcp Pd_2Au sites is not possible (see also section 3.3). This is included in the values given in Table 1. In that case we have to subtract all Pd_2 or Pd_2Au sites on Pd_2 dimers from the total number of Pd_2 bridge sites or Pd_2Au hollow sites. On the other hand, adsorption on the Pd_2Au sites above a linear Pd_3 trimer or at both sides of a compact Pd_3 trimer would per se be possible. Due to the pairwise adsorption discussed above, a linear Pd_4 ensemble can accommodate only two rather than three H_{ad} species on Pd_2 or Pd_2Au sites. Finally, we may assume that a certain minimum size of the Pd_n ensemble is required for hydrogen adsorption, the critical Pd_n ensemble size. The concentrations of Pd_2 or Pd_2Au sites on the different

surface alloys resulting from the different restrictions described above (no occupation of directly neighbored bridge sites or Pd_2Au threefold hollow sites, pairwise adsorption only, and adsorption only on ensembles with a certain minimum size) are listed in the lines 3-6 and 8-11 in Table 1. Similar arguments can also be constructed for adsorption on Pd_3 hollow sites, where a compact trimer would be able to accommodate only a single H_{ad} species. The resulting concentrations of Pd_3 sites are also listed lines 13 and 14 in Table 1.

Finally, we will consider blocking effects. We can reasonably assume that adsorption on Pd_3 hollow sites is more stable than on Pd_2 bridge sites or on Pd_2Au threefold hollow sites (see also section 3.3). On the other hand, a H adatom adsorbed on a Pd_3 site will block the directly neighboring Pd_2Au sites or Pd_2 bridge sites for H adsorption, and vice versa. In this case we assume that it is energetically more favorable to adsorb two H_{ad} on Pd_2Au sites (or on Pd_2 bridge sites) than one H_{ad} on a Pd_3 site. For adsorption on larger ensembles this would lead to the following consequences: First, recombinative desorption of 2 H_{ad} species on two Pd_3 sites in one ensemble occurs in the β_2 peak, similar to desorption from a Pd(111) surface. Second, the preference for adsorption of more H_{ad} species means that if a Pd_n surface ensemble contains one or two Pd_3 sites which due to site blocking effects are not populated at H_{ad} saturation coverage, they will become occupied after partial desorption of H_{ad}, by migration of H_{ad} from weaker bonding sites to strongly bonding Pd_3 sites, once site blocking is not effective any more. Desorption of two H_{ad} species on two Pd_3 sites will not contribute to the β_1 peak any more. Hence, these H_{ad} species have to be subtracted from the total amount of adsorbed H_{ad} when calculating the β_1 desorption intensity. For instance, if an ensemble would be able to accommodate 4 H_{ad} on Pd_2Au sites or alternatively 2 H_{ad} on Pd_3 sites, where in the latter case the Pd_2Au sites are blocked for H_{ad}, we assume that this Pd_n ensemble would adsorb 4 H_{ad}. After desorption of the first H_2 molecule, the remaining H_{ad} species change to

the two Pd_3 sites and do not contribute to the desorption intensity in the β_1 peak. If only one Pd_3 site is available, one may debate whether desorption from one Pd_2Au (or Pd_2) site and one Pd_3 site occurs in the β_1 or in the β_2 peak. We here assume the latter, the number of such cases is, however, so small that they will not cause significant modifications in the β_1 desorption intensity. These effects were considered in the calculated desorption intensities listed in the last lines 16 and 17 for Pd_2 bridge sites and Pd_2Au threefold hollow sites, respectively.

Inspection of the resulting concentrations of the different adsorption ensembles and the hydrogen uptake in the β_1 state at 120 K indicates that even after consideration of these additional restrictions for hydrogen adsorption on the different PdAu bimetallic surfaces the concentration of active and accessible Pd_2 and Pd_2Au adsorption sites is sufficient to explain the desorption intensity in the β_1 peak, indicating that the underlying mechanistic ideas of a pairwise adsorption on a Pd_n ensemble and of a certain minimum size of the Pd_n adsorption ensemble are correct. In combination with the conclusions described already above, the experimental findings result in the following model for hydrogen adsorption on a PdAu/Pd(111) surface alloy:

1. Surface diffusion of H_{ad} species between different Pd_n ensembles is inhibited, while surface diffusion between sites within the individual Pd_n adsorption ensemble is assumed to be facile.

2. The confinement of the H_{ad} species to the original Pd_n adsorption ensemble results in a pairwises adsorption and desorption behavior on the individual Pd_n ensembles, and in significant deviations from a second order desorption kinetics typical for H_2 desorption.

3. Accordingly, adsorption of hydrogen is determined by the size and shape of the individual Pd_n adsorption ensembles. Desorption in the β_1 state is related to H adatoms adsorbed on

sites which allow for bridge bonded CO adsorption, i.e., adsorption on Pd_2 sites or on Pd_2Au threefold hollow sites. Adsorption on atop sites in general and on Pd monomers in particular is inhibited. Adsorption on Pd_3 threefold hollow sites is tentatively associated with desorption in the β_2 peak.

4. Based on the quantitative comparison between H_{ad} uptake in the β_1 state and the concentrations of different adsorption sites and ensembles (see Table 1), Pd ensembles with at least 4 Pd atoms seem to be the smallest ensembles to allow dissociative adsorption of hydrogen at 100 K, indicating that the critical Pd cluster size for hydrogen adsorption on dispersed PdAu surface alloys under these conditions is a Pd_4 tetramer (see also below). Because of the very low (compact Pd_3 ensembles) or even extremely low (compact Pd_4 tetramer sites) surface concentrations of compact trimers and tetramers, hydrogen adsorption has to be possible on linear or bent Pd_n (with $n \geq 4$) ensembles.

5. Neither from the abundance of the different adsorption sites and their variation with Pd surface concentration nor from the HREELS data we can unambiguously differentiate between adsorption on Pd_2 bridge sites or on Pd_2Au threefold hollow sites, although based on the general preference of adsorbed hydrogen for threefold hollow sites the latter seems to be more reasonable.

These ideas derived from the experimental data shall be tested and compared with predictions based on theory in the next section.

3.3 Theoretical description of the interaction of hydrogen with PdAu/Pd(111) surface alloys

H adsorption in a (2x2) unit cell: For elucidating trends, we calculated the adsorption energies for a variety of adsorption sites on different Pd_xAu_{4-x}/Pd(111) surface alloys in a

(2×2) unit cell with 1, 2, or 3 Pd atoms on the surface layer and 1 hydrogen atom per unit cell. For comparison, hydrogen adsorption on a Pd(111) surface was also included. As mentioned earlier, we will focus on trends rather than on absolute values when comparing the calculated adsorption energies. The adsorption sites and the related adsorption energies are illustrated in Fig. 7.

For adsorption on Pd(111), the adsorption energies decrease in the order fcc site > bridge site >> atop site (Fig. 7). The difference of ~1 eV between fcc site and atop site agrees well with results of recent calculations.[64] Going from Pd(111) to the surface alloys, we expect the following trends for adsorption on the Pd surface atoms based on predictions from the d-band model and from the experimental findings for other bimetallic adsorption systems. First, due to strain effects (compression of the Pd surface atoms by the larger Au atoms in the pseudomorphic surface layer) we expect bonding on the Pd surface atoms to be weaker than on Pd(111). Second, due to the chemical interaction with neighboring Au atoms and the weaker Pd-Au interaction as compared to Pd-Pd interaction, we expect the adsorbate – Pd bond to be stronger on the surface alloys than on Pd(111) ('bond order conservation'). Since these two effects are counteracting, a simple decision on the actual trends is not possible from these qualitative arguments, underlining the need for detailed calculations.

We relate the hydrogen adsorption energy to two properties of the adsorption site. One is the composition of the site, which is associated with the nature of the ensemble ('ensemble effect'). The other is the surrounding of the site, where the composition of the site remains fixed. This reflects the (lateral) ligand effect. The DFT results show that the hydrogen adsorption on PdAu/Pd(111) is not as strong as that on Pd(111) (Fig. 7), even at the sites with similar compositions, e.g., Pd_3 hollow, Pd_2 bridge and Pd_1 atop sites. The weakened H-Pd interaction can be well explained by the downward shift of Pd d-band center upon formation

of the surface alloy with Au. According to our previous calculations,[36] increasing the Au content in the surface from, 0.25 ML to 0.75 ML increases the downshift of the Pd d-band center. As a result, the hydrogen adsorption energy decreases upon going from hollow site 4 to hollow site 18 (Fig. 7). In addition, according to the DFT calculations hydrogen prefers to bind with Pd rather than with Au surface atoms. The higher the Pd content of the adsorption ensemble, the stronger the corresponding hydrogen binding. For the sites involving of the same number of Pd atoms, hydrogen favors three-fold hollow sites (Pd_3 and Pd_2Au sites) rather than bridge and atop sites. Accordingly, in the following calculations for PdAu/Pd(111) containing Pd monomers, dimers and trimers (see below), only hydrogen adsorption at the stable hollow sites was considered. The only exception is the adsorption on the $PdAu_2$ hollow sites, which is slightly less stable than that on Pd-Au bridge site (site 11 vs. 12; site 15 vs. 17, Fig. 7).

H adsorption in a (3x3) unit cell: In a next step we performed comparative calculations in a (3×3) unit cell with a low H_{ad} coverage (θ_H = 0.11 ML) and Pd surface contents of 1, 2, 3 and 4 Pd surface atoms per unit cell. It allows us to model small Pd surface ensembles such as monomers, dimers, trimers and tetramers that are fully surrounded by Au surface atoms, as the observed experimentally (see Fig. 8). As evident from Fig. 8, the adsorption energy increases from $PdAu_2$ hollow adsorption at a Pd_1 monomer to the Pd_2Au hollow at a Pd_2 dimer and to finally adsorption on a Pd_3 hollow site on a compact Pd_3 trimer. This increase in adsorption energy reflects the ensemble effect. In this case, the only variable is the composition of the adsorption ensemble, which is fully surrounded by Au in the first shell (Fig. 8). On the other hand, the adsorption on the Pd_3 hollow site on a compact Pd_3 trimer in Fig. 8 is significantly less stable than adsorption on the Pd_3 hollow on a compact Pd_4 tetramer. These two sites differ just by the atoms in the shell around the Pd_3 hollow, where 9 Au atoms surround the Pd_3 trimer compared to 8 Au and 1 Pd surface atoms are for the case of the Pd_4 tetramer (Fig. 8).

Accordingly, the corresponding energy difference reflects the influence of electronic ligand effects, as the first shell surrounding of the adsorption site varies from one site to the next, while the composition of the adsorption site ('adsorption ensemble') remains identical. According to our calculations, the d-band center of Pd shifts toward the Fermi level from -2.74 eV for a Pd_1 monomer via -2.67 eV and -2.61 eV for a compact Pd_3 trimer, respectively, to -2.58 eV for a compact Pd_4 tetramer, where the changes in the initial three values arise from the ensemble effect, and the last one from the decreasing Au coordination in the first ligand shell. In comparison, H adsorption on a threefold hollow site on Pd(111), where all surface atoms in the first ligand shell are Pd atoms and the d-band center of Pd is located at -2.16 eV, is significantly stronger. The stabilization of H_{ad} with decreasing Au coordination in the first ligand shell means that the (stabilizing) strain effects dominate, and are stronger than (destabilizing) lateral ligand effects. Similar effects are observed for adsorption on Pd_2 bridge sites or Pd_2Au hollow sites, where adsorption at an isolated Pd_2 dimer is significantly less favorable than adsorption on a similar site on / aside a string of Pd surface atoms (Fig. 9). These examples further underlines the role of electronic ligand effects in hydrogen interaction with PdAu/Pd(111) surface alloys.

Both ligand and ensemble effects result in an approximately linear correlation between the surface composition and the hydrogen adsorption energy; which is illustrated in Fig. 8b. As mentioned before, however, the variation in hydrogen binding energy introduced by the ligand effect is not as significant as that by the ensemble effect.

To assess and further elucidate the influence of strain and vertical ligand effects, we performed similar calculations on a pseudomorphic PdAu surface alloy supported on a Au(111) substrate. According to the simple rules given above we would expect the H-Pd bond to be stronger in this case because of the larger lattice constant of Au compared to Pd(111) via adding tensile strain on the pseudomorphic PdAu monolayer (strain effect), and because of the

weaker Pd-Au interaction compared to the Pd-Pd interaction via directly strengthening the H-Pd bond (vertical electronic ligand effect). The results are illustrated in Fig. 8b. As expected, the adsorption energies are generally larger than those obtained for PdAu/Pd(111), reflecting the effect of strain and vertical ligand effects. The trends for the (in plane) ensemble effect and the (lateral) ligand effect, which are illustrated by the dashed line, are qualitatively similar to those observed on PdAu/Pd(111), with the energies for adsorption on the three ensembles following a linear relation whose slope differs only little from that determined for adsorption on PdAu/Pd(111). We will get back to these results at the end of this section, when comparing with electrochemical experiments performed on PdAu/Au(111) surface alloys.

Overall, the DFT calculations show that at a mixed adsorption site the adsorption energy can be affected by both ensemble and ligand effects, where the effect is more pronounced for the ensemble effect, but the ligand effect is also sizable. These findings agree well with the trends derived for the adsorption of CO, O and N on similar surfaces.[36]

2H adsorption in (3x3) and (3x4) unit cells: In a third step we calculated the adsorption energies for adsorption of 2 H atoms per ensemble for $Pd_{1\text{-}4}$ ensembles, again mostly in a (3×3) unit cell, to include the effect of pairwise adsorption discussed above (Fig. 10). A (3×4) unit cell was also included to model a linear Pd_3 trimer isolated by Au, which was observed using STM. Also here we find a clear trend, with adsorption becoming increasingly more stable on going from a Pd_1 monomer to a Pd_4 tetramer. Similar to the results for adsorption of a single H atom, the adsorption on atop sites on the Pd_2 dimer is significantly less stable than adsorption on the closely neighbored Pd_2Au sites (fcc and hcp site). The markedly lower adsorption energy of the latter configuration compared to that on other, larger ensembles, however, fully justifies the assumption made when setting up the adsorption-desorption model from correlating the STM and TPD data in section 3.2, where we had excluded adsorption of 2 H adatoms on neighbored fcc and hcp sites.

Similar as in the case of a Pd_2 dimer, the adsorption of 2 H atoms also prefers the two Pd_2Au sites of a compact Pd_3 trimer, the binding is, however, significantly stronger than on the same sites on a Pd_2 dimer (Fig. 10). As discussed above, the difference in adsorption energy at the same Pd_2Au site composition reflects the ligand effect, which is associated with the variation in the surrounding of the site. In addition, the repulsion due to the closer proximity of the two H_{ad} species on the Pd_2 than on the Pd_3 ensemble also contributes to the weaker hydrogen adsorption, since the distance between two H_{ad} atoms is shorter on the Pd_2 dimer (1.65 Å) than on the Pd_3 trimer (2.81 Å). Finally, a configuration with one H_{ad} located in the central Pd fcc site of the compact Pd_3 trimer and the other one in the directly neighbored hcp site is slightly less stable by 0.02 eV than the adsorption on the two Pd_2Au sites of that ensemble (Fig. 10). Obviously, the repulsion between the closely spaced H adatoms overcompensates the energy gain from having one H_{ad} adsorbed on the more stable Pd_3 site.

The most stable adsorption among the different Pd_n ensembles considered is obtained for adsorption on a compact Pd_4 tetramer. In this case, the configuration with 2 H_{ad} on the Pd_3 sites is most stable, despite of the close proximity of the directly neighbored fcc and hcp adsorption sites (Fig. 10). Obviously, the energy gain upon having two H adatoms located on Pd_3 sites overcompensates the repulsion between the closely neighbored H_{ad} species.

For better comparison of the absolute adsorption energies with the experiment, we re-calculated the adsorption energies of some representative configurations using larger slabs and allowing relaxation of the topmost two metal layers (see section 2.2). The resulting energies are given in brackets for these ensembles in Fig. 10. They essentially confirm the trends derived from the calculations described before, and they furthermore yield adsorption energies which fit reasonably well to the experimental data also on an absolute scale. Interestingly, the adsorption of 2 H atoms on the two Pd_2Au sites of a compact Pd_3 trimer is slightly less stable

than that on the Pd_2Au sites above a linear Pd_3 trimer (Fig. 10). In this case, the compositions of the adsorption sites (Pd_2Au) and their surrounding (8 Au and 1 Pd) are identical and 2 H_{ads} are packed in a similar position, sharing 1 Pd atom. Our calculations show that the small difference in hydrogen binding (0.15 eV) is associated with different strain in the two Pd_3 ensembles, where the compact Pd_3 introduces a higher compressive strain within the Pd_3 (0.7%) and therefore a weaker hydrogen binding than the linear Pd_3. Different from the experimental data, our calculations suggest that a linear or compact Pd_3 trimer is the smallest Pd ensemble, allowing the dissociative adsorption of hydrogen both energetically (adsorption energy -0.27 eV on a linear Pd_3 ensemble). Calculations of the activation barrier for dissociative H2 adsorption on a linear Pd_3 trimer yielded a value of 0.4 eV. Possible explanations for the apparent discrepancy between theory and experiment will be discussed below.

Overall, the trends derived from the calculations agree very well with the conclusions from the combined STM and TPD data (see adsorption model in section 3.2); furthermore they allowed us to distinguish between adsorption sites and configurations where this was not possible from our experimental data: The calculations clearly confirm that adsorption on Pd monomers and dimers as well as on atop sites are unfavorable, justifying the corresponding assumptions we had made for the determination of the adsorbate coverage from the ensemble size distributions (see Table 1). The strongly antibinding adsorption on Au_3 sites fully supports the assumption of pairwise hydrogen adsorption and ensemble confinement of the H adatoms, since it is energetically more favorable for H_{ad} to desorb by recombination with a second H_{ad} than to move to a Au_3 site, where the latter would be the first step to surface diffusion to another Pd_n ensemble. Furthermore, the calculations favor the adsorption on Pd_2Au sites as compared to Pd_2 bridge sites, which we had favored before (see section 3.2), but where clear proof could not be provided. The only point where experimental finding and

calculations seem to disagree is the critical ensemble size, where from calculations Pd_3 ensembles should be sufficient to stabilize hydrogen adsorption, while experimental data tend to favor Pd_4 tetramers as critical ensemble size. Here it should be noted this does not refer to compact Pd_4 tetramers and the tetramer sites, whose number is far too small to explain the intensity in the β_1 peak, but to linear or bent Pd_4 tetramers. This discrepancy may result from two effects: first considering that on an absolute scale the differences in calculated β_1 peak intensity between a Pd_3 and Pd_4 critical ensemble size are still small, experimental errors, e.g., in the coverage determination of the β_1 peak may be possible; second the adsorption energy on the Pd_3 trimers may be too low to populate these sites at 100 K and to stabilize hydrogen adsorption up to the onset of desorption in the β_1 peak at around 150 K. Considering the significant ligand effect determined for this adsorption system (compare, e.g., adsorption on Pd_2Au sites on a Pd_2 dimer and on a Pd_n chain in Fig. 9) and the higher repulsions between H_{ad} on neighbored Pd_2Au sites, the increase in stability for adsorption on Pd_4 and larger ensembles as compared to adsorption on Pd_3 ensembles may indeed be sufficient to stabilize hydrogen adsorption on Pd_4 and larger Pd_n ensembles under the present experimental conditions, while stable adsorption on linear or bent Pd_3 ensembles would be inhibited. Furthermore, the calculated barrier for dissociative adsorption on a linear Pd_3 trimer of 0.4 eV means that the sticking probability is so low ($s_0 < 10^{-17}$ at 110 K) that during a normal adsorption experiment these sites would not be populated.

Finally it should be noted that the present findings and interpretation agree very well also with findings from an electrochemical study, investigating hydrogen adsorption on a PdAu/Au(111) surface alloy, which was prepared *in-situ* by diffusion limited codeposition of Pd and Au on a Au(111) substrate to yield a mixed AuPd monolayer of defined composition.[49] In that study, Pd_2 dimers (or Pd_2Au trimers) were identified as smallest Pd ensemble which is

able to adsorb hydrogen. For electrochemical experiments in acidic solution (hydrogen underpotential deposition - H_{upd}), hydrogen is supplied by H^+ species from the electrolyte, and therefore the need for locally accommodating 2 H_{ad} species does not exist. Furthermore, the observation that hydrogen adsorbed on Pd_2Au sites is stable against desorption as H_2 (from adsorption ensembles with more than 1 H_{ad}) also at room temperature, in contrast to the onset of desorption from these sites at <200K on PdAu/Pd(111) (see Fig. 3), can at least partly be explained by the different substrate (Au(111) rather than Pd(111)). The different lattice constants and the different chemical nature of the two substrates result in tensile rather than compressive strain and weaker vertical ligand effects, which in turn lead to a stabilization of the metal-hydrogen bonds (see Fig. 8b). Furthermore, recombinative desorption from Pd_2 dimers (with one adsorbed hydrogen atom) would not be possible. Desorption as H^+, in contrast, is mainly controlled by the adsorption potential.

In a more general sense the present findings for hydrogen adsorption and desorption on PdAu/Pd(111) can be considered as representative for adsorption and reaction on bimetallic surfaces where one surface species shows a very low adsorption energy for the respective adsorbate and where ensemble effects are dominant, but ligand effects are still effective. In that case, the activity of the surface will rapidly decrease with increasing surface concentration of the weakly binding surface species. On the other hand, the large variety of different adsorption sites on different ensembles means that the surface activity is tunable. According to the Sabatier principle, there will always be an ensemble, which can provide the optimal adsorption for maximizing their activity for a catalytic process reaction. In that case, careful optimization of the surface composition opens the possibility to optimize the activity of the bimetallic catalyst.

4 Conclusions

The structure and local hydrogen adsorption properties of disordered PdAu/Pd(111) surface alloys were studied in a combined experimental and theoretical approach, aiming at a quantitative description of the overall adsorption properties in a coherent microscopic picture, in terms of local chemisorption properties of individual metal nanostructures. Employing high resolution STM imaging and TPD as well as HREELS measurements on the one hand and periodic density functional theory calculations on the other hand, we arrive at the following conclusions:

1) In the PdAu/Pd(111) surface alloys, which were formed by annealing a (partly) Au covered Pd(111) surface, Pd and Au surface atoms are homogeneously distributed over the surface, and their distribution follows essentially a random distribution, indicative of weak net interaction energies between the two species. For up to 20% Pd surface concentration, Pd surface atoms are arranged predominantly as monomers and dimers, and only at higher Pd surface concentration larger ensembles contribute measurably.
2) Correlation of desorption intensities in TPD spectra with the abundance of different adsorption ensembles and adsorption sites for different Pd surface concentrations indicates that Pd_4 tetramers are the smallest ensemble ('critical ensemble') that can adsorb hydrogen via dissociative adsorption of H_2, with H adsorption taking place on Pd_2Au threefold hollow sites under present adsorption conditions (UHV, 120 K). Calculations find stable adsorption already on the same sites on Pd_3 trimers, but the adsorption energy may be too low to allow adsorption at 120 K, in addition, adsorption on these sites is hindered by a sizable activation barrier.
3) Hydrogen adsorption on PdAu/Pd(111) surface alloys exhibits a pronounced ensemble effect, being most stable on Pd_3 threefold hollow sites, less stable on Pd_2 bridge sites and least stable on Pd monomers. HREELS measurements as well as DFT data indicate that adsorption on Pd_2Au sites is more favorable than adsorption on Pd_2 bridge sites. Lateral

(in plane) ligand effects in contrast are smaller due to two opposing effects: increasing the number of Pd atoms in the surface alloys reduces the tensile strain which should increase the local adsorption strength, but it also increases the interaction with neighboring Pd atoms which decreases the local reactivity of the respective Pd surface atom. Both effects partly cancel each other for PdAu/Pd(111) surface alloys.

4) The formation of 2 desorption peaks at 235 K and 325 K, respectively, which is observed for H_2 desorption from surfaces with Pd surface concentrations of 20% - 40%, is attributed to desorption from a weakly bound state where the H adatoms are not adsorbed in a Pd_3 threefold hollow site, but on a Pd_2Au site, or where the two Pd_3 sites are directly neighbored fcc and hcp Pd_3 sites, e.g., for compact tetramers. Accordingly, the higher temperature desorption peak is tentatively attributed to desorption from 2 Pd_3 sites with at least 1 lattice constant separation.
5) Surface diffusion of H adatoms between isolated Pd_n ensembles is inhibited due to the high energy of H_{ad} adsorbed on Au_3 surface sites, i.e., the H adatoms are confined to the original Pd_n adsorption ensemble. As a consequence, dissociative adsorption of H_2 molecules is only possible if both H_{ad} species can be stable adsorbed on the same Pd_n ensemble, and hydrogen adsorption occurs pairwise.

Overall, these results illustrate the detailed insight into the chemistry of bimetallic surfaces accessible from such kind of combined experimental and theoretical model studies on structurally well defined surfaces, and we expect these trends to be valid in a more general sense for comparable adsorption systems. Applying similar approaches to reaction studies will be the next task.

Acknowledgements

We gratefully acknowledge a fellowship of the Alexander von Humboldt Foundation (AvH)

for N.T and financial support by the Deutsche Forschungsgemeinschaft via the Research Unit 1376 (Be 1201/18-2). The DFT calculations were performed with support from the Danish Center for Scientific Computing through grant no.HDW-1101-05.

References

1. J. H. Sinfelt, *Surf. Sci.*, 2002**, 500**, 923.
2. P. T. Wouda, B. E. Nieuwenhuys, M. Schmid and P. Varga, *Surf. Sci.*, 1996**, 359**, 17.
3. F. Buatier de Mongeot, M. Scherer, B. Gleich, E. Kopatzki and R. J. Behm, *Surf. Sci.*, 1998**, 411**, 249.
4. P. Varga, M. Schmid, *Appl. Surf. Sci.* , 1999**, 141**, 287.
5. J. A. Rodriguez, D. W. Goodman, *Acc. Chem. Res.*, 1995**, 28**, 477.
6. B. Hammer, J. K. Nørskov, *Adv. Catal.*, 2000**, 45**, 71.
7. A. Gross, *Theoretical Surface Science - A Microscopic Perspective*, Springer, Berlin, 2nd Edition ed. 2009**,** 1.
8. J. K. Nørskov, F. Abild-Pedersen, F. Studt and T. Bligaard, *Proc. Natl. Acad. Sci. U. S. A.*, 2011**, 108**, 937.
9. F. Besenbacher, I. Chorkendorff, B. S. Clausen, B. Hammer, A. M. Molenbroek, J. K. Nørskov and I. Stensgaard, *Science*, 1998**, 279**, 1913.
10. N. M. Markovic, T. J. Schmidt, V. Stamenkovic and P. N. Ross, *Fuel Cells*, 2001**, 1**, 105.
11. J. Greeley, J. K. Nørskov, *J. Phys. Chem. C*, 2009**, 113**, 4932.
12. M. Chen, D. Kumar, C.-W. Yi and D. W. Goodman, *Science*, 2005**, 310**, 291.
13. M. S. Chen, K. Luo, T. Wei, Z. Yan, D. kumar, C. W. Yi and D. W. Goodman, *Catal. Today*, 2006**, 117**, 37.
14. P. Han, S. Axnanda, I. Lyubinetsky and D. W. Goodman, *J. Am. Chem. Soc.*, 2007**, 129**, 14355.
15. T. Wei, J. Wang and D. W. Goodman, *J. Phys. Chem. C*, 2007**, 111**, 8781.
16. M. Chen, D. W. Goodman, *Chin. J. Catal.*, 2008**, 29**, 1178.
17. F. Gao, D. W. Goodman, *Chem. Soc. Rev.*, 2012**, 41**, 8009.
18. B. Gleich, M. Ruff and R. J. Behm, *Surf. Sci.*, 1997**, 386**, 48.
19. M. Ruff, S. Frey, B. Gleich and R. J. Behm, *Appl. Phys. A*, 1998**, 66**, S513.
20. M. Ruff, N. Takehiro, P. Liu, J. K. Nørskov and R. J. Behm, *ChemPhysChem*, 2007**, 8**,

2068.

21. R. J. Behm, *Z. Phys. Chem.*, 2009**, 223**, 9.
22. V. Ponec, W. M. H. Sachtler, *J. Catal.*, 1972**, 24**, 250.
23. J. H. Sinfelt, J. J. Carter and D. J. C. Yates, *J. Catal.*, 1972**, 24**, 283.
24. T. Bligaard, J. K. Nørskov, *Electrochim. Acta*, 2007**, 52**, 5512.
25. M. Mavrikakis, B. Hammer and J. K. Nørskov, *Phys. Rev. Lett.*, 1998**, 81**, 2819.
26. Y. Soma-Noto, W. M. H. Sachtler, *J. Catal.*, 1974**, 32**, 315.
27. W. M. H. Sachtler, G. A. Somorjai, *J. Catal.*, 1983**, 81**, 77.
28. H. Conrad, G. Ertl and E. E. Latta, *Surf. Sci.*, 1974**, 41**, 435.
29. M. Beutl, J. Lesnik, *Vacuum*, 2001**, 61**, 113.
30. G. E. Gdowski, T. E. Felter and R. H. Stulen, *Surf. Sci.*, 1987**, 181**, L147.
31. T. E. Felter, R. H. Stulen, M. L. Koszykowski, G. E. Gdowski and B. Garrett, *J. Vac. Sci. Technol. A*, 1989**, 7**, 104.
32. M. Beutl, J. Lesnik, *Surf. Sci.*, 2001**, 482-485**, 353.
33. B. Hammer, J. K. Nørskov, *Nature*, 1995**, 376**, 238.
34. A. G. Sault, R. J. Madix and C. T. Campbell, *Surf. Sci.*, 1986**, 169**, 347.
35. C.-W. Yi, K. Luo, T. Wei and D. W. Goodman, *J. Phys. Chem. B*, 2005**, 109**, 18535.
36. P. Liu, J. K. Nørskov, *Phys. Chem. Chem. Phys.*, 2001**, 3**, 3814.
37. D. D. Eley, *J. Res. Inst. Catalysis, Hokkaido Univ.*, 1967**, 16**, 101.
38. C. J. Baddeley, R. M. Ormerod, A. W. Stephenson and R. M. Lambert, *J. Phys. Chem.*, 1995**, 99**, 5146.
39. C. J. Baddeley, M. Tikhov, C. Hardacre, J. R. Lomas and R. M. Lambert, *J. Phys. Chem.*, 1996**, 100**, 2189.
40. H. C. Ham, G. S. Hwang, J. Han, S. W. Nam and T. H. Lim, *J. Phys. Chem. C*, 2009**, 113**, 12943.
41. H. C. Ham, J. A. Stephens, G. S. Hwang, J. Han, S. W. Nam and T. H. Lim, *Catal. Today*, 2011**, 165**, 138.
42. J. K. Edwards, A. Thomas, B. E. lsona, P. Landon, A. F. Carley and G. J. Hutchings,

Catal. Today, 2007 **, 122**, 397.

43. R. C. Tiruvalam, J. C. Pritchard, N. Dimitratos, J. A. Lopez-Sanchez, J. K. Edwards, A. F. Carley, G. J. Hutchings and C. J. Kiely, *Faraday Discuss.*, 2011**, 152**, 63.
44. M. Neurock, D. Mei, *Top. Catal.*, 2002**, 20**, 5.
45. Y. Pluntke, L. A. Kibler and D. M. Kolb, *Phys. Chem. Chem. Phys.*, 2008**, 10**, 3684.
46. J. A. Meier, K. A. Friedrich and U. Stimming, *Faraday Discuss.*, 2002**, 121**, 365.
47. J. Meier, J. Schiøtz, P. Liu, J. K. Nørskov and U. Stimming, *ChemPhysLett*, 2004**, 390**, 440.
48. S. Pandelov, U. Stimming, *Electrochim. Acta*, 2007**, 52**, 5548.
49. F. Maroun, F. Ozanam, O. M. Magnussen and R. J. Behm, *Science*, 2001**, 293**, 1811.
50. J. K. Nørskov, T. Bligaard, A. Logadottir, J. R. Kitchin, J. G. Chen, S. Pandelov and U. Stimming, *J. Electrochem. Soc.*, 2005**, 152**, J23.
51. A. Roudgar, A. Groß, *Phys. Rev. B* , 2003**, 67**, 033409.
52. A. Roudgar, A. Gross, *J. Electroanal. Chem.*, 2003**, 548**, 121.
53. A. Roudgar, A. Gross, *Surf. Sci.*, 2004**, 559**, L180.
54. M. Ruff, PhD thesis, Ulm University, 2000.
55. This code is available under https://wiki.fysik.dtu.dk/dacapo.
56. D. Vanderbilt, *Phys. Rev. B*, 1990**, 41**, 7892.
57. B. Hammer, L. B. Hansen and J. K. Nørskov, *Phys. Rev. B*, 1999**, 59**, 7413.
58. T. A. Halgren, W. N. Lipscomb, *Chem. Phys. Lett.*, 2014**, 49**, 225.
59. W. A. Hofer, G. Ritz, W. Hebenstreit, M. Schmid, P. Varga, J. Redinger and R. Podloucky, *Surf. Sci.*, 1998**, 405**, L514.
60. H. E. Hoster, A. Bergbreiter, P. Erne, T. Hager, H. Rauscher and R. J. Behm, *Phys. Chem. Chem. Phys.*, 2008**, 10**, 3812.
61. H. Conrad, G. Ertl and E. E. Latta, *Surf. Sci.*, 1974**, 43**, 462.
62. P. Nordlander, J. K. Nørskov and F. Besenbacher, *J. Phys. F:Met. Phys.*, 1986**, 16**, 1161.
63. H. Conrad, M. E. Kordesch, R. Scala and W. Stenzel, *J. Electron Spectrosc. Relat. Phenom.*, 1986**, 38**, 289.

64. L. Mancera, L, R.J. Behm, and A. Groß, to be published

Table I

Relative abundance of different adsorption sites evaluated from the sets of STM images for the three Pd surface concentrations used also for the D_2-TPD and HREELS measurements (values relative to Pd(111).

No.	Adsorption Site	$Pd_{21}Au_{79}$ / %	$Pd_{28}Au_{72}$ / %	$Pd_{38}Au_{62}$ / %
1	Pd_1 sites[1]	21	28	38
2	Pd_2 sites	7.4	13.7	25.0
3	Pd_2 sites without Pd_2 dimers[2]	4.5	10.7	23,4
4	Pd_2 sites without Pd_2 dimers and Pd_3 trimers[3]	2.5	8.2	22.1
5	Pd_2 sites without Pd_2 dimers, only pairwise occu Pation[4]	4.1		
6	Pd_2 sites without Pd_2 dimers and Pd_3 trimers, only pairwise occupation[4]	2.0	7.1	20.7
7	Pd_2Au sites	8.1	12.0	30.0
8	Pd_2Au sites without Pd_2 dimers[2]	5.4	12.0	28.5
9	Pd_2Au sites without Pd_2 dimers and Pd_3 trimers[3]	2.8	9.2	8,2
10	Pd_2Au sites without Pd_2 dimers, only pairwise occupation[4]	4.6	11.0	27.1
11	Pd_2Au sites without Pd_2 dimers and Pd_3 trimers, only pairwise occupation[4]	2.3	8.2	25.4
12	Pd_3 sites	0.5	0.8	4.5
13	Pd_3 sites without Pd_3 trimers[3]	0.3	0.6	4.3
14	Pd_3 sites without Pd_3 trimers, with pairwise occupation[5]	0.1	0.2	3.0
15	Compact Pd_4 sites	<0.1	<0.1	0.9
16	D_2 desorption (β_1 peak) from Pd_2 sites without Pd_2 dimers and trimers as calculated from the adsorption sites.[6]	3.7	9.9	21.2
17	D_2 desorption (β_1 peak) from Pd_2Au sites without Pd_2 dimers and Pd_3 trimers as calculated from the adsorption sites.[6]	1.9	7.1	19.8
18	D_2 desorption in β_1 peak	1.2±0.3	5.0±1.0	14.5±1.5

[1] Concentration of Pd_1 sites is identical to the total concentration of Pd surface atoms.

[2] Concentration of the respective sites without considering those in Pd_2 dimers.

[3] Concentration of the respective sites without considering those in Pd_2 dimers and Pd_3 trimers.

[4] Concentration of the respective sites without considering those in Pd_2 dimers and assuming that only even numbers of H adatoms can be adsorbed from H_2 adsorption (no H_{ad} spill-over between ensembles).

[5] Concentration of the respective sites without considering those in Pd_3 trimers, and assuming that only even numbers of H adatoms can be adsorbed from H_2 adsorption (no H_{ad} spill-over between ensembles).

[6] Calculation and assumptions see text.

Figure Captions

Figure 1 STM images of Pd-Au bimetallic surfaces with atomic and chemical resolution with different amounts of Pd in the surface layer: a) 3.5% Pd, b) 12% Pd, c) 23% Pd and d) 78% Pd (a) 130 Å × 130 Å, 3.3 ML Au, 5 min annealed at 680 K; b) 135 Å × 135 Å, 2.6 ML Au, 1 min at 700 K; c) 83 Å × 83 Å, 2.6 ML Au, 1 min at 825 K; d) 145 Å × 145 Å, 0.3 ML Au, 30 s at 775 K.

Figure 2 Abundance of compact 2-, 3-, 4- and 5-fold ensembles as a function of Pd-surface concentration. The composition of ensembles is as denoted in the legends, the actual positions of the Pt and Au atoms within the ensembles are not explicitly considered. Symbols result from STM data, lines denote calculated distribution for a purely random distribution.

Figure 4 Series of D_2 TPD spectra recorded upon increasing the D_2 exposure up to saturation on the $Pd_{38}Au_{62}$ surface alloy (exposures are given in L, with 1 L = 1.33 × 10^{-6} mbar s).

Figure 3 Series of D_2 TPD spectra recorded upon saturation of surface alloys with increasing Pd content in the topmost layer: $Pd_{21}Au_{79}$, $Pd_{28}Au_{72}$, $Pd_{38}Au_{62,}$ Pd(111).

Figure 5 HREEL spectra of the $Pd_{38}Au_{62}$ surface exposed to 4 L of H_2 (a) at 120 K and (b) at room temperature.

Figure 6 Series of D_2 TPD spectra in the CO titration experiment on the $Pd_{21}Au_{79}$ surface. The sample was first exposed to 0.5 L of CO at 140 K, then annealed to the temperature indicated, cooled down to 120 K and exposed to D_2. (a) CO TPD spectrum, (b) D_2 TPD spectrum without annealing, c) – g) D_2 TPD spectra recorded after annealing to (c) 330 K, (d) 360 K, (e) 380 K, (f) 400 K and (g) 430

K.

Figure 7 Hydrogen adsorption energies at different sites on a Pd(111) surface and on Pd_xAu_{4-x}/Pd(111) sites in a (2×2) unit cell. Left panel: Schematic presentation of the different surfaces and of the various adsorption sites: Pd(111): sites 1 – 3, Pd_3Au/Pd(111): sites 4 – 8, Pd_3Au/Pd(111): sites 9 – 14, and Pd_3Au/Pd(111): sites 15 – 18 (adsorption energies in eV per H_2 molecule).

Figure 8 Effect of the composition of the Pd_xAu_{3-x} adsorption ensemble (a) for adsorption on a threefold hollow site on a PdAu/Pd(111) surface alloy (b). Adsorption ensembles as indicated in the a). Red line corresponds to the ensemble effect; black line describes the ligand effect. For comparison and to illustrate the role of strain and vertical ligand effect, we also included the adsorption energies calculated in the same way and for the same sites on a PdAu/Au(111) surface alloy (dashed lines).

Figure 9 Illustration of the ligand effect and the ensemble effect for H adsorption on a Pd_2 bridge site and a Pd_2Au threefold hollow site of a PdAu/Pd(111) surface alloy.

Figure 10 Adsorption energies for simultaneous adsorption of 2 H adatoms as expected for dissociative adsorption of H_2 without spillover of H_{ad} to other Pd_n ensembles (Pd_2 dimer, Pd_3 compact trimer and Pd_4 compact tetramer) on a PdAu/Pd(111) surface alloy as illustrated in the figure.

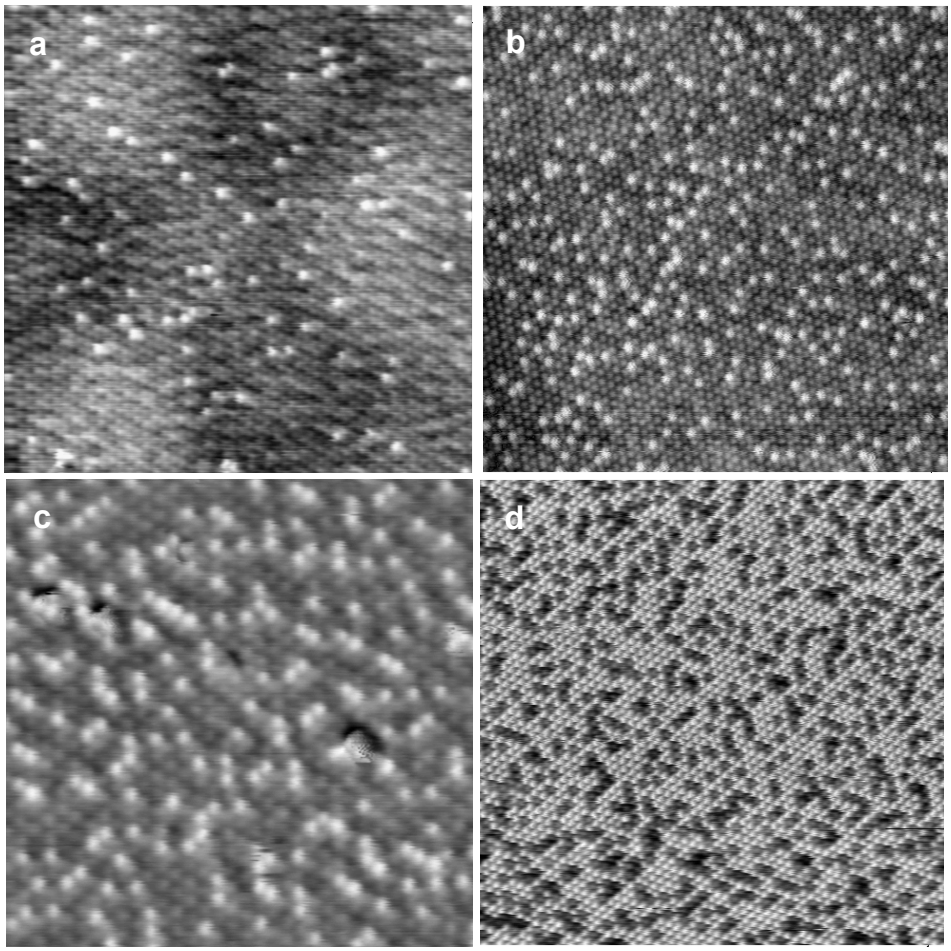

Figure 1 N. Takehiro et al.

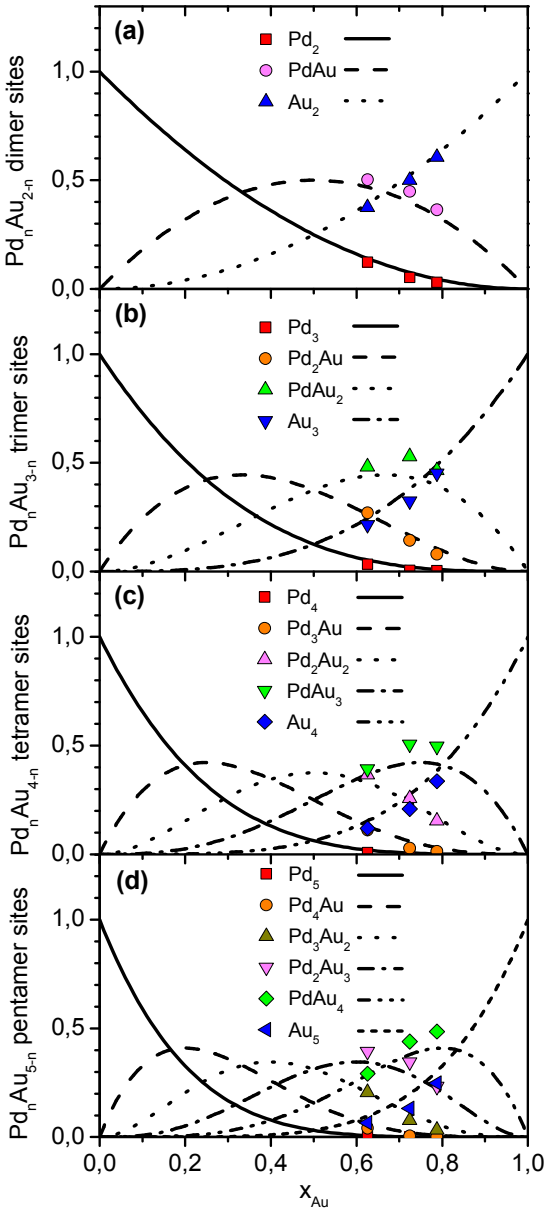

Figure 2 N. Takehiro et al.

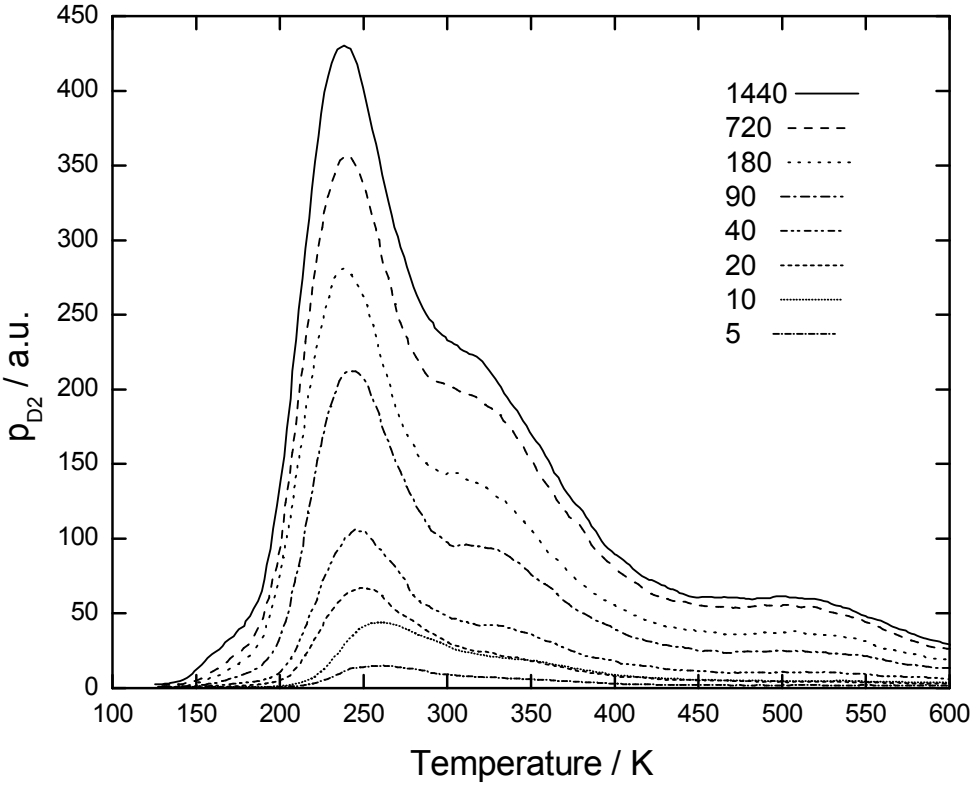

Figure 3 N. Takehiro et al.

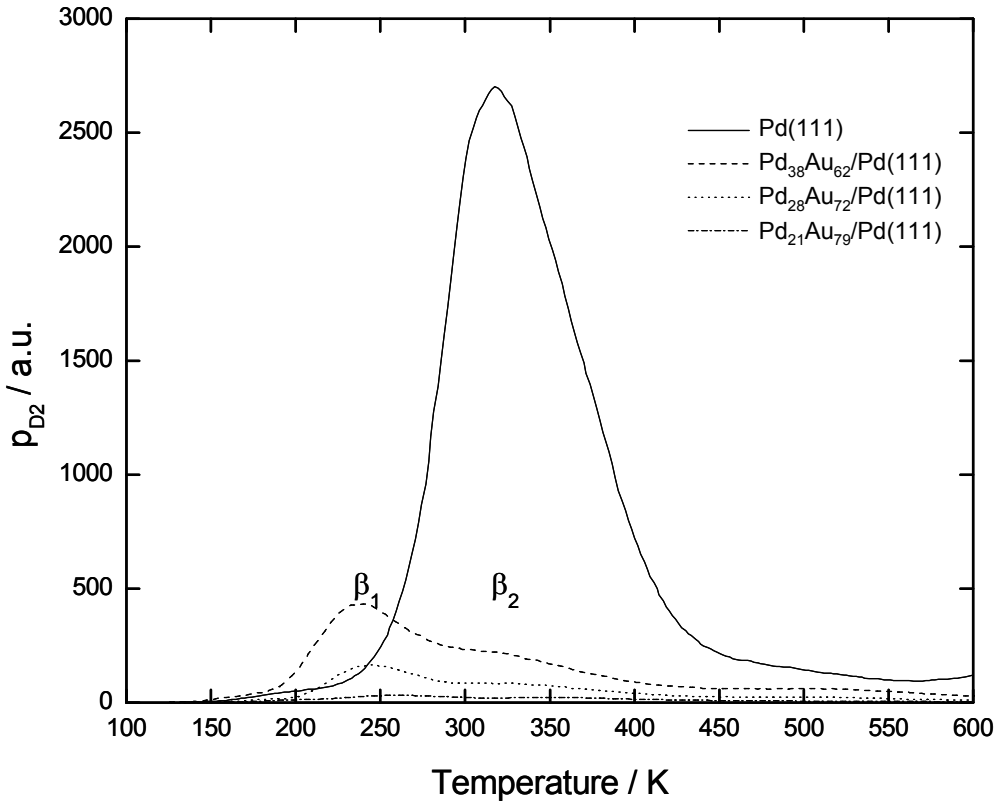

Figure 4 N. Takehiro et al.

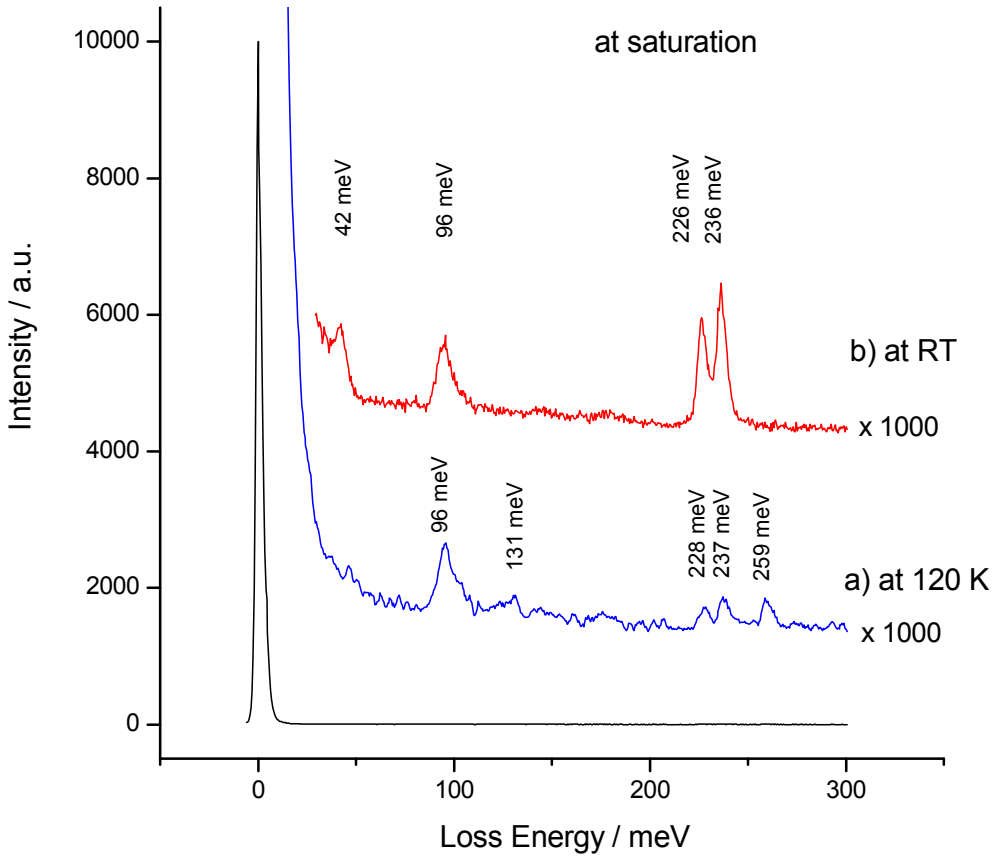

Figure 5 N. Takehiro et al.

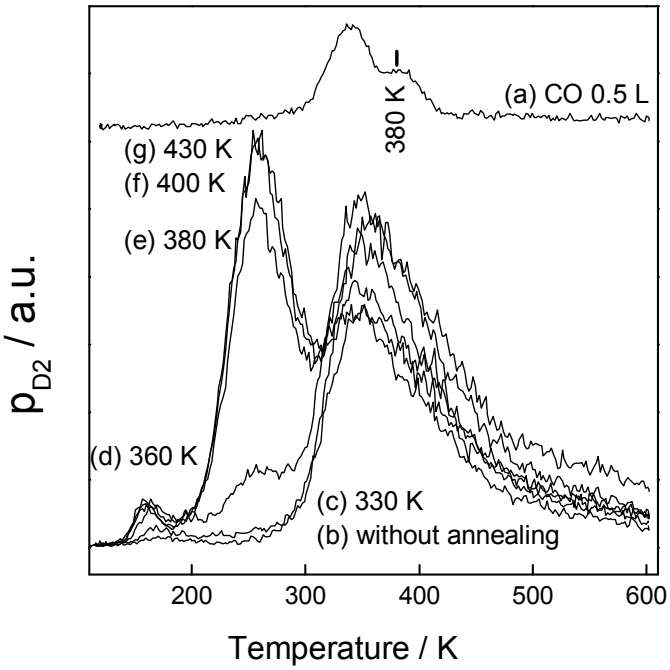

Figure 6 N. Takehiro et al.

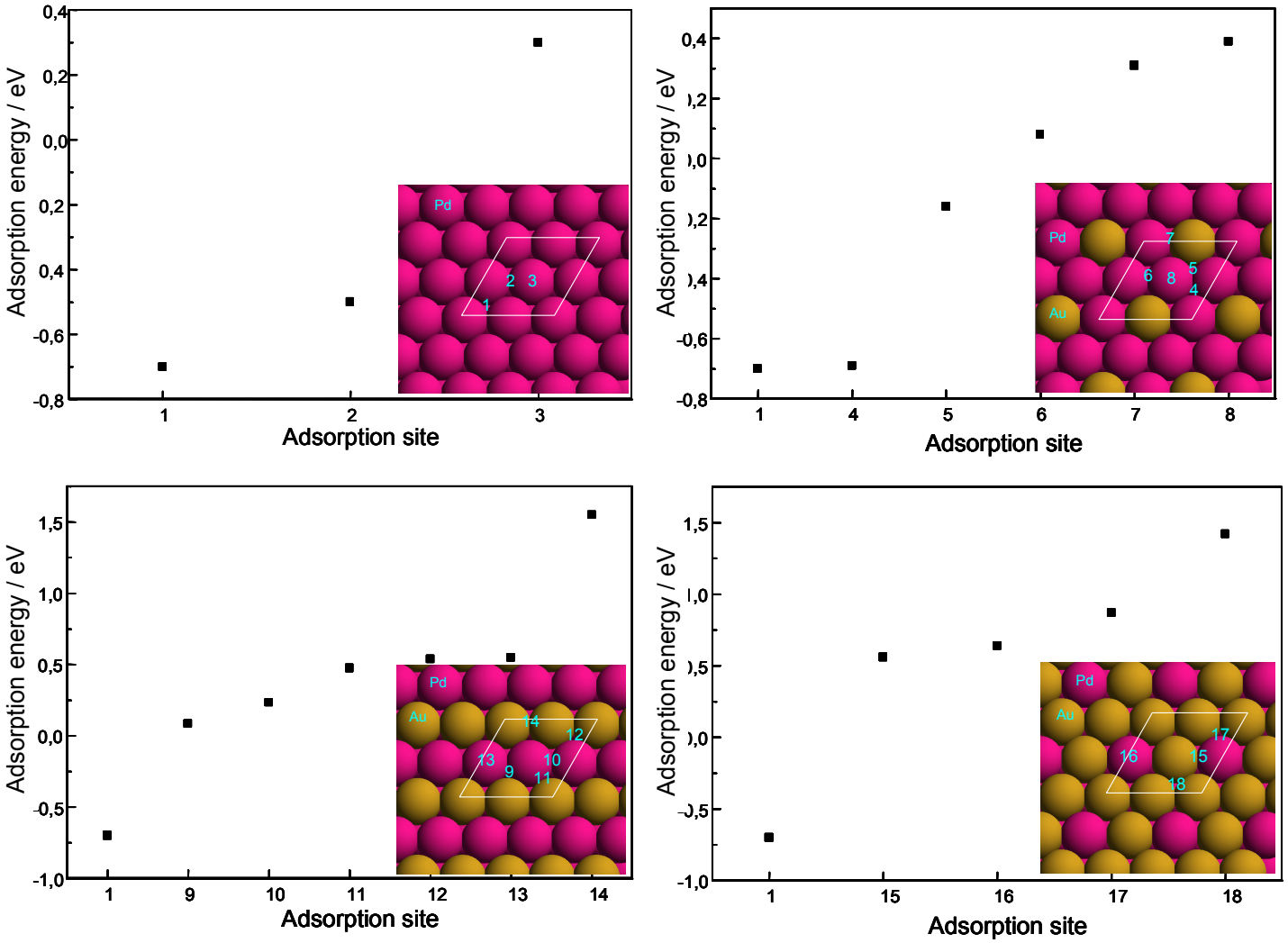

Fig. 7

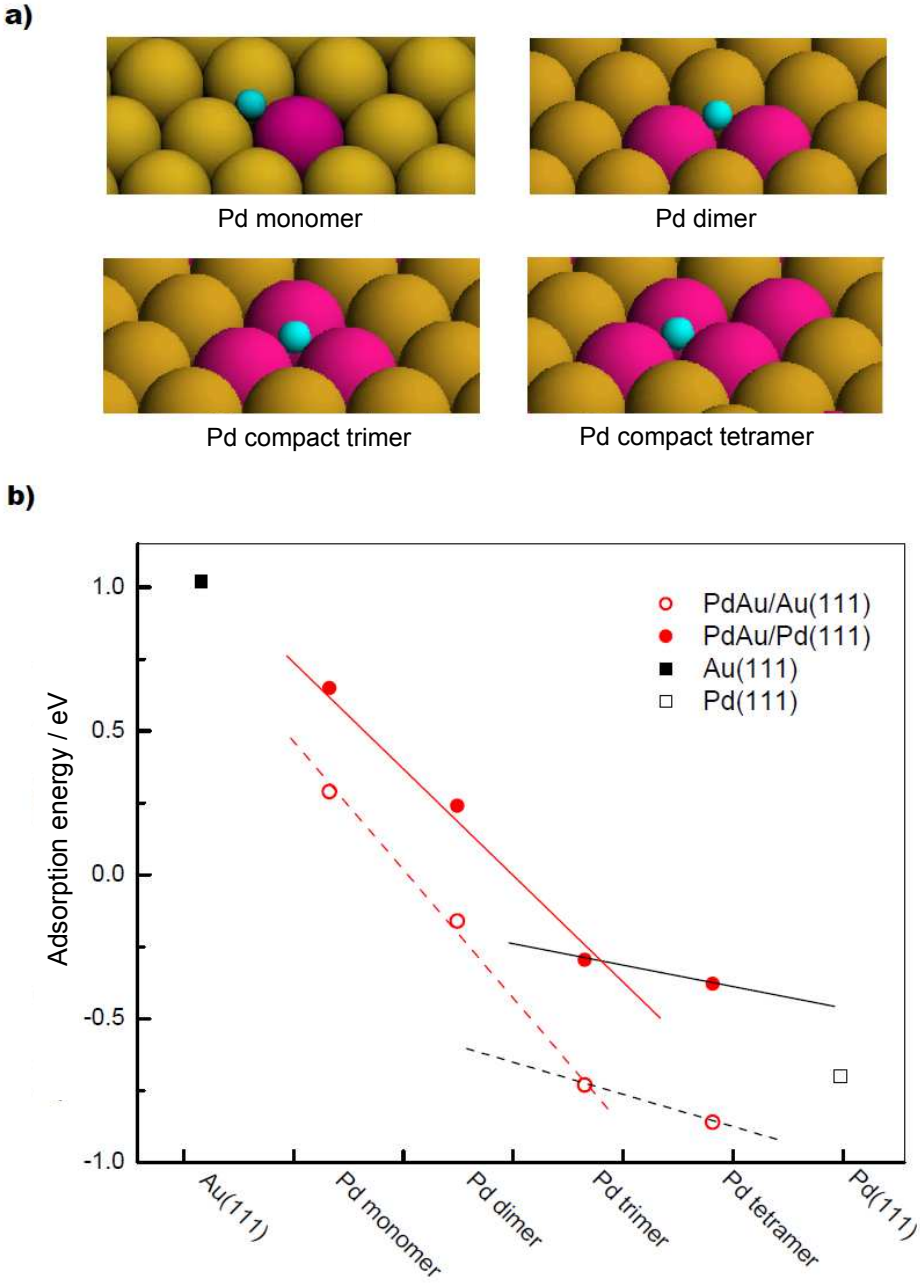

Fig. 8 N. Takehiro et al.

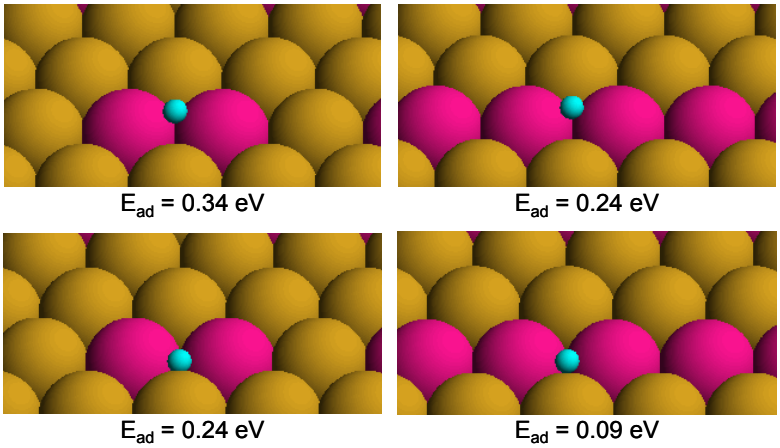

Fig. 9 N. Takehiro et al.

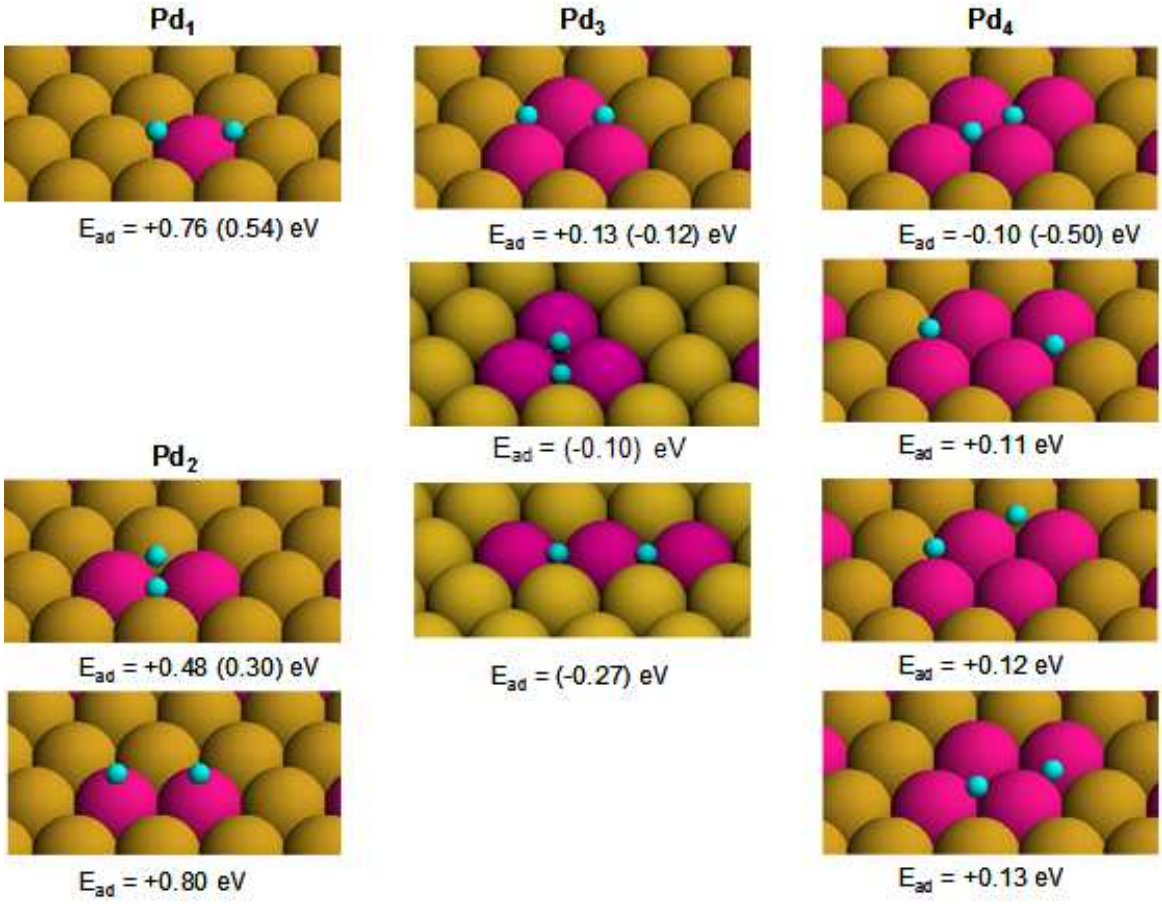

Fig. 10 N. Takehiro et al.

Graphical Contents Entry

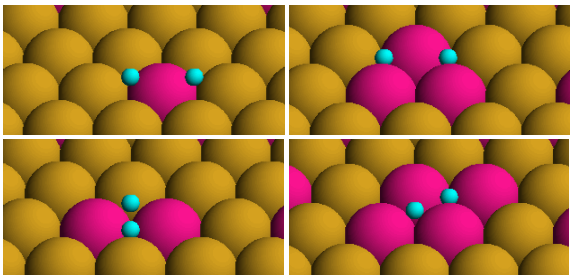

Microscopy and spectroscopy measurements in combination with periodic DFT calculations provide detailed insight into the adsorption behavior of hydrogen on disordered, but structurally well defined PdAu/Pd(111) surface alloys, finding this to be dominated by a distinct ensemble confinement of the H_{ad} and geometric ensemble effects, while electronic strain and lateral ligand effects partly compensate each other and are less significant.